CHAPTER 3

SYNTHESIS AND CHARACTERIZATION OF *INSITU* FORMED ZrB_2 REINFORCED ZA COMPOSITES

3.1 INTRODUCTION

This chapter deals with the synthesis of ZrB_2 reinforced/ZA composites with different Vol.% of ZrB_2 particles by the direct melt reaction (DMR) *insitu* technique. The reaction between reactants was studied to find out the temperature of formation of ZrB_2 particles. The ZA/ZrB_2 composites have been characterized by different techniques and the influence of varying vol.% of ZrB_2 particles on microstructure, physical, and mechanical properties of ZA composites is presented and discussed in coming sections.

3.2 CHEMICAL COMPOSITION OF THE COMPOSITES

Chemical composition of composites was evaluated by chemical extraction method and is given in Table 3.1. This table shows theoretical and actual vol.% of ZrB_2 while actual composition of the base alloy remains same.

Table 3.1 Theoretical and actual vol.% of ZrB_2 in composites

Composites	Vol.% ZrB_2	
	Theoretical	Actual
ZA/0 Vol.% ZrB_2	0	0
ZA/3 Vol.% ZrB_2	3	2.89
ZA/4.5 Vol.% ZrB_2	4.5	4.35
ZA/6 Vol.% ZrB_2	6	5.60
ZA/9 Vol.% ZrB_2	9	8.37

3.3 XRD ANALYSIS

XRD analysis was conducted for all four composite samples. Cu-Kα radiation (wavelength, λ=1.5406 Å), scan at the rate of 10° min^{-1} was used for phase identification. Figure 3.1 represents the XRD patterns of test materials. β (Zn) with HCP crystal structure and α (Al) with FCC crystal structure are the primary phases [Berent et al., 2016]. The composites exhibit extra peaks of ZrB_2 along with the phases of the matrix alloy. This confirms the formation of ZrB_2 within the melt. This can also be seen as the vol.% of ZrB_2 increases the intensity of ZrB_2 peaks also increases. Apart from Zn, Al and ZrB_2, no other peaks were present which is indicative of completion of reaction [Vineet et al., 2019]. It also ensures that another likely phases such as Al_3Zr and AlB_2 are not formed.

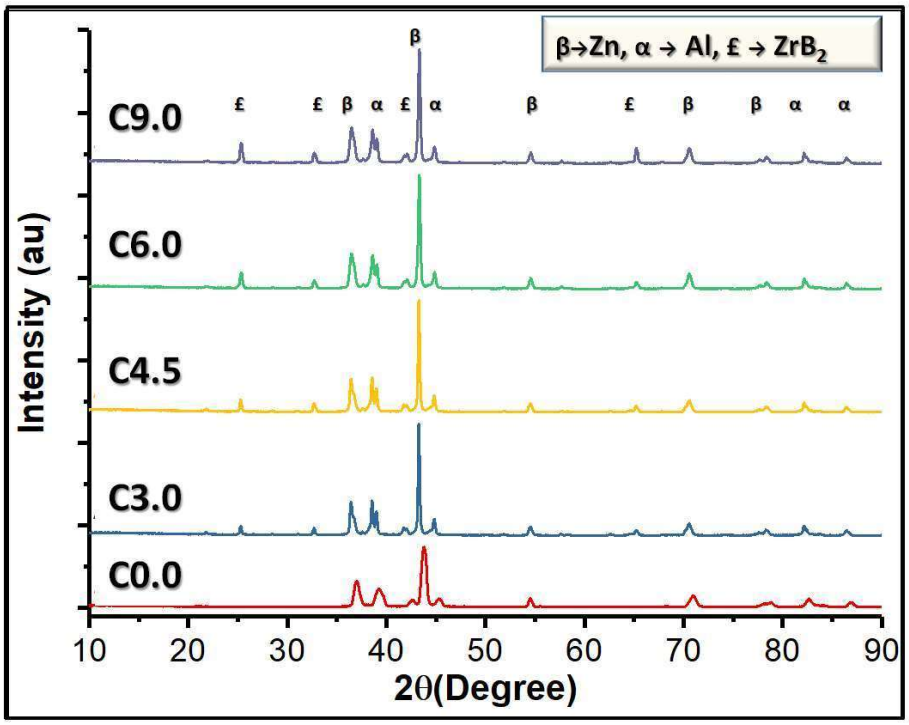

Fig. 3.1 XRD pattern of ZA alloy and composites

3.4 DENSITY AND POROSITY DETERMINATION

The experimental densities (evaluated by Archimedes principle) and porosity (determined using equation 2.6) of ZA alloy and composites are given in Fig. 3.2 (a & b). However, it is observed that with increasing amount of ZrB_2 (Fig 3.2(a)) there is slight decrease in density which looks contrary as density of ZrB_2 (6.08×10^3 kg m^{-3}) is higher than the density of ZA alloy (4.94×10^3 kg m^{-3}). Further, it is observed from Fig 3.2(b) that with increase in vol.% of ZrB_2 particles in the matrix porosity tends to increase, which causes density decrease in the composites with increased amount of ZrB_2. Stirring of the melt causes vortex formation in the melt which creates pressure zone difference. This pressure difference entraps the air. Though degasser has been used but it seems it is not able to take care of longer reaction times. There is mismatch in the coefficient of thermal expansion of matrix and ZrB_2, which creates thermal gradient during the solidification in different regions. Such regions increase with higher amount of ZrB_2 and higher gas entrapment causing increase in porosity.

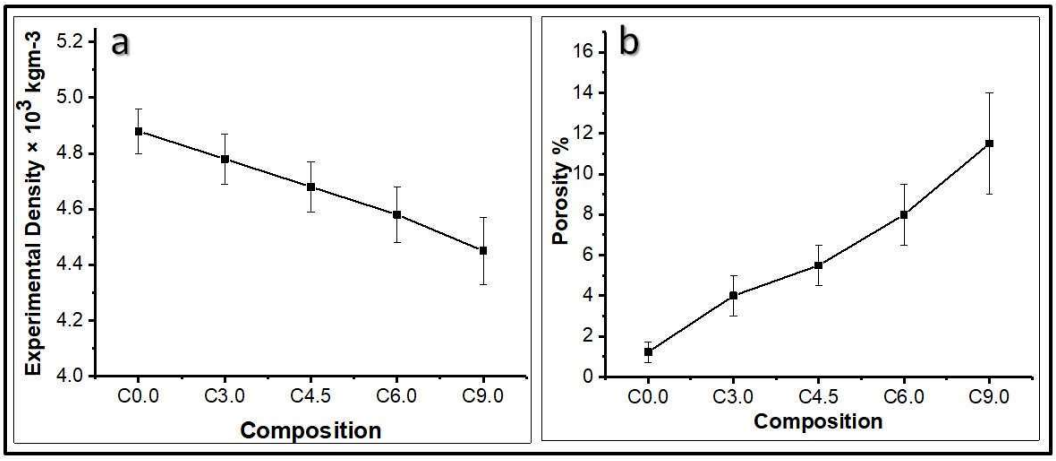

Fig. 3.2 (a) Experimental densities (b) Porosity % of ZA alloy and composites

3.5 OPTICAL MICROSCOPY

Figure 3.3 presents the OM image C0.0 alloy, C3.0, C4.5, C6.0 and C9.0 composites. ZA alloy exhibits a dendritic structure consisting of Al rich (α phase) surrounded by α+β eutectic phase and Zn rich (β phase) (Fig. 3.3(a)). Al is the primary alloying element in Zn-based alloys and influences solidification behaviour and microstructure of the alloy. Addition of Al into Zn imparts fluidity and also refines its grains and results in increase in strength of the alloy [Apelian et al., 1981]. The microstructure of Zn-Al alloys is mixture of α-phase (dark black colour shown by red arrow), β-phase (light colour shown by red arrow) and α+β eutectic phase (grey colour shown by red arrow).

ZA alloy based composites shows similar microstructure with reinforcement of ZrB_2 particles. The OM image of composites with 3, 4.5, 6 and 9 vol.% of ZrB_2 are given in Fig. 3.3(b-e). These figures indicate homogeneous distribution of ZrB_2 particles. Incorporation of ZrB_2 particles in matrix shows significant reduction in the dendrites. Further, as content of ZrB_2 rises from 3 to 9 vol.%, the grain size reduces significantly as it can be seen from Fig. 3.3 (b) to (e). The average grain size of the alloy and composites were also calculated according to ASTM standard E112 from optical micrographs to have further clarity and are given in Fig. 3.4.

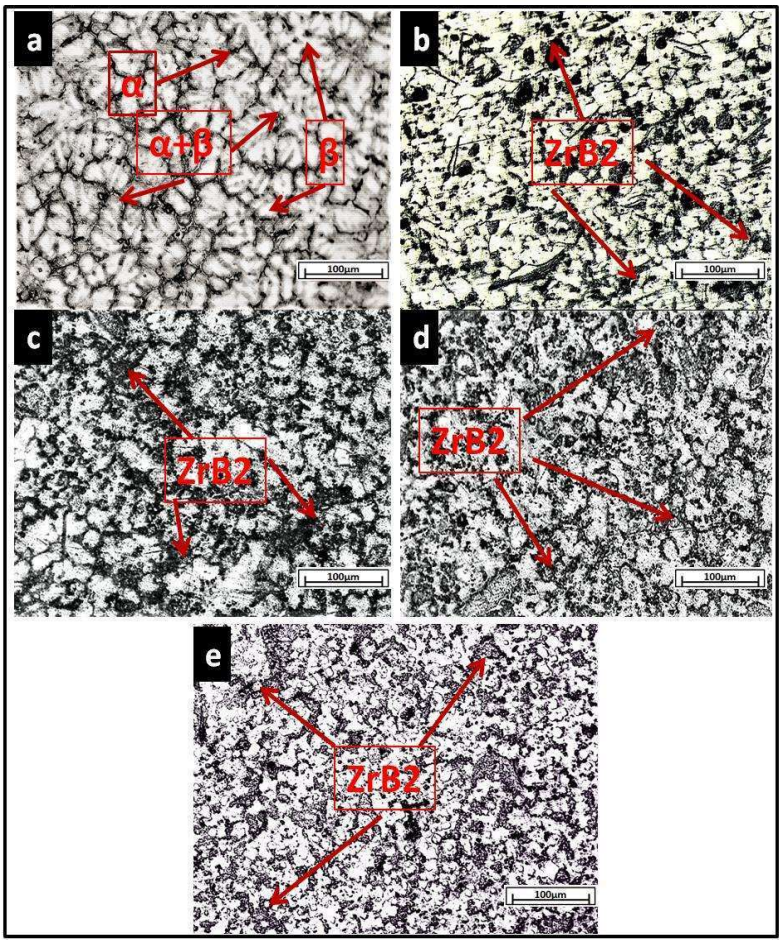

Fig. 3.3 Optical microstructure image of (a) C0.0 (b) C3.0 (c) C4.5 (d) C6.0 and (e) C9.0

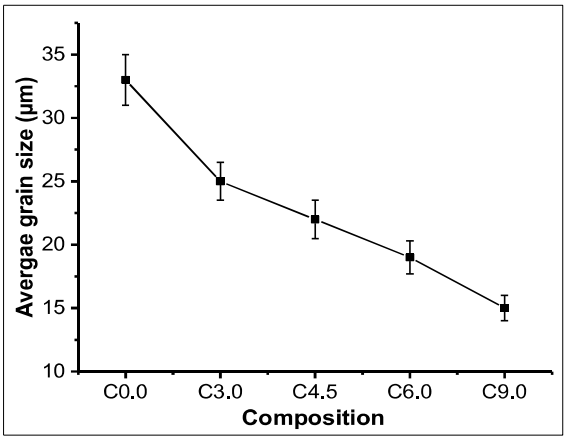

Fig. 3.4 Average grain size of ZA alloy and composites

From the Fig. 3.4, it can be clearly seen that the grain size of matrix alloy refined from 33.0 ± 2.0 μm to 15.0 ± 1.0 μm for C9.0 composite. ZrB_2 behaves as nucleation sites for matrix grains and also restricts the movement of solidification front, which leads to refinement of grains of composites resulting in improvement in mechanical properties, that in turn impacts the tribological properties of composites [Gautam et al., 2015].

3.6 SCANNING ELECTRON MICROSCOPY

SEM studies of composite materials were conducted to have clarity in morphology including distribution of ZrB_2 particles. SEM micrographs in Fig. 3.5 show mostly uniform distribution of *insitu* formed ZrB_2 particles in ZA matrix for all composites with different vol.% of ZrB_2 particles. SEM micrographs (Fig. 3.5(e)) shows hexagonal shape ZrB_2 particles. EDS analysis of composites (Fig 3.6) also confirm presence of only Al, Zn and Zr (boron is not detectable by SEM due to very low atomic number), which further confirms the *insitu* formation of only ZrB_2 particles. Particle size distributions of ZrB_2 particles has also been evaluated using SEM micrographs. Figure 3.7 shows the ZrB_2 particle size histogram for all the composites. This is also evident from Fig. 3.7(a)–(d) that number of particles are more at higher compositions, however, clustering effect is also pronounced with increasing number of particles [Ramesh et al., 2019, Han et al., 2019]. This can be seen from the Fig. 3.7 that the size of ZrB_2 particles varies within a range of 0.1 μm to 1.3 μm for different composites. Most of the particles are within a range of 0.3 to 0.9 μm.

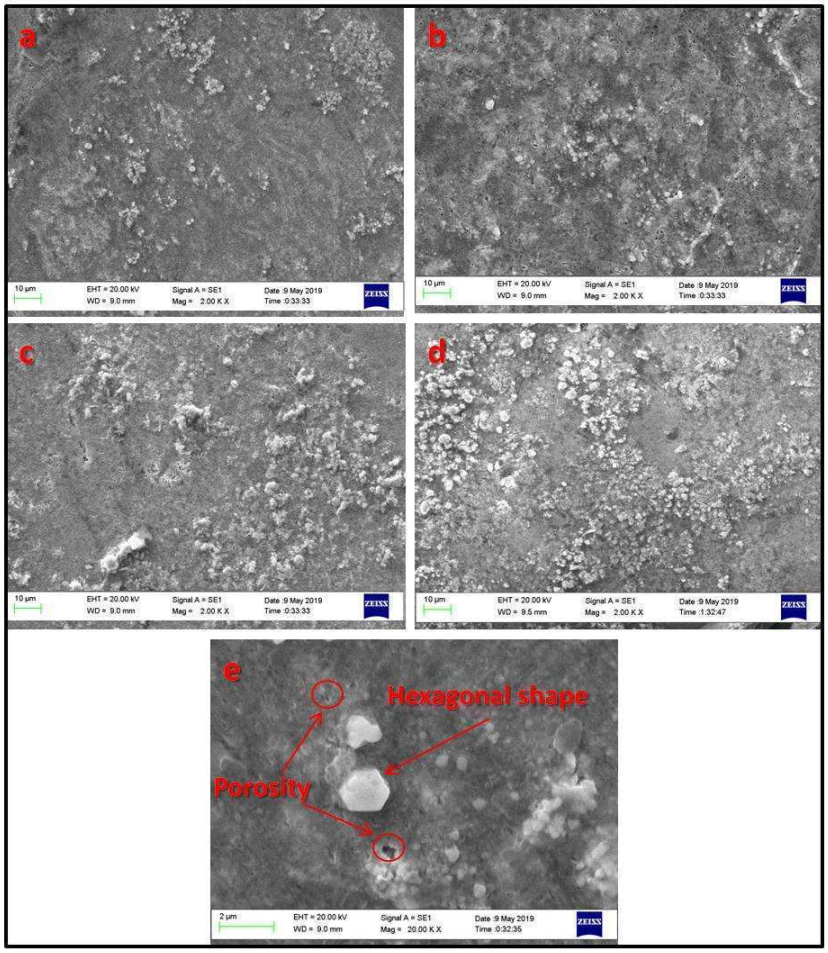

Fig. 3.5 Scanning electron micrographs of composites with different vol.% of ZrB_2 particles (a) C3.0 (b) C4.5 (c) C6.0 (d) C9.0, and (e) morphology of ZrB_2 particles

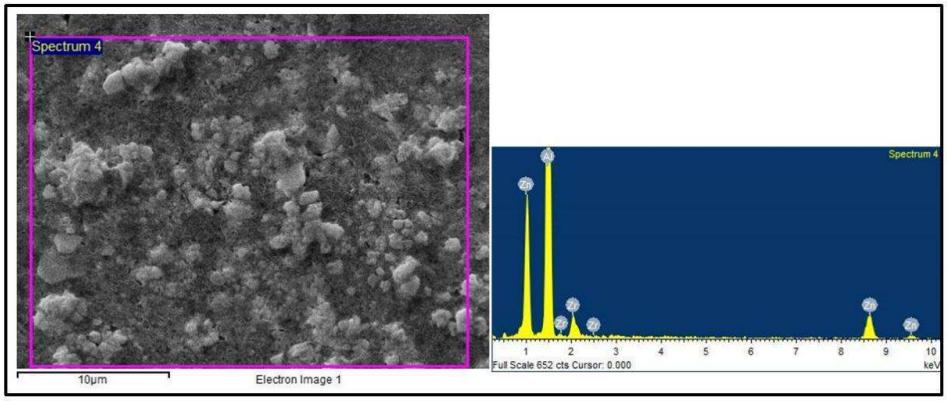

Fig. 3.6 EDS of the C9.0 composites

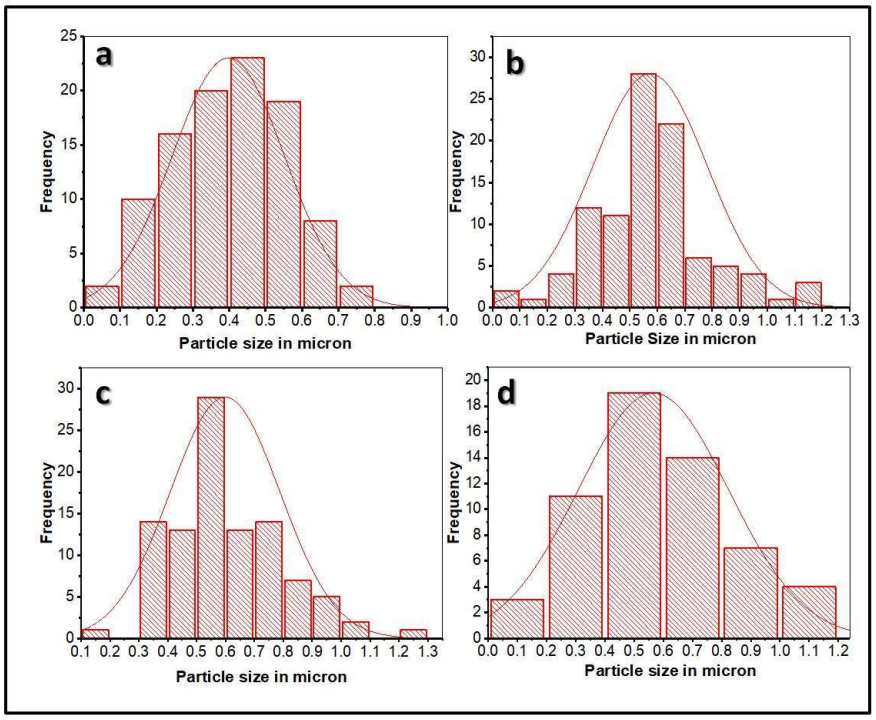

Fig. 3.7 ZrB_2 particle size distribution of (a) C3.0 (b) C4.5 (c) C6.0 (d) C9.0

3.7 MECHANICAL BEHAVIOUR OF ZA ALLOY AND COMPOSITES

Figure 3.8 presents the stress strain curve, % elongation, tensile strength, yield strength while Fig. 3.9 exhibits compressive strength and hardness of the alloy and composites. As content of ZrB_2 reinforcement increases from 0 vol.% to 9 vol% there is significant increase in tensile strength (Fig. 3.8(c)), compressive strength (Fig. 3.9(a)) and hardness (Fig. 3.9(b)) but at the expense of ductility (Fig. 3.8(b)). This increase in mechanical properties greatly influences the tribological properties of composites. Grain refinement, Orowan strengthening mechanism and dislocations generation caused increase in above stated properties in the composite (Gautam et al., 2015). The reciprocity interaction between grain boundaries and dislocations led to strengthening of composites due to increased lattice disorder and misorientation of grains at grain boundaries. This lattice

disorder and misorientation causes the hindrance in the movement of dislocations and enhances the strength of composites. The presence of ZrB_2 particles act as second phase in the composites and refine grains of the matrix, which can be clearly understood from Fig. 3.3 and Fig. 3.4. As the content of ZrB_2 increases, the hindrance in propagation of dislocation also increases and further refined grain size of the composites resulted and an increase in strength of composites is observed [Gautam et al., 2015]. The propagation of dislocation is further hindered due to generation of loops throughout the reinforced particles owing to the finer size (less than 0.9 μm) in composites as it bows and then reconnect resulting a rise in strength of the composites [Aqida et al., 2012]. The effect of generation of loops is more as vol.% of ZrB_2 increases.

In the composites, the volumetric strain is generated due to mismatch in CTE among matrix and reinforcement particle during the course of solidification, which helps in the growth of dislocations close to particles and enhances the flow stress in the matrix [Tavakoli et al., 2007]. Formation of dislocation plays key role in improving hardness of composites. Variation in CTE of alloy and reinforced particles in the course of solidification has led to formation of these dislocations. Additionally, presence of the hard ZrB_2 particles also enhances the hardness of composites. The high strength of the composites confirms wettability between the matrix alloy and the *insitu* formed ZrB_2 particles. Similar kind of observations were also reported by Gautam et al., in the TEM analysis of metal matrix composites consisting of ZrB_2 particles. % elongation (ductility) of composites decreases due to the existence of hard ZrB_2 particles as their amount increases ductility is adversely affected. Further, clustering of the reinforced particles may also contribute during the course of testing and could have caused generation of voids, where cracks may nucleate and

propagate, resulting in premature failure and reduced ductility [Yalcin et al., 2018, Guler et al., 2019].

The Compressive strength of ZA alloy and composites has been evaluated at ambient temperature and variation of compressive strength with composition is shown in Fig. 3.9(a) as bar diagram. As the ZrB_2 content is increased, the compressive strength of the composites also increases. This increase in compressive strength may be attributed to reduction in matrix grain size, uniformly distributed harder ZrB_2 particulates into the ductile matrix, mismatch in thermal expansion coefficient causing dislocations. Load transfer from matrix to particles also plays a key role. Orowan strengthening effect is another cause of strengthening in composites. Presence of ZrB_2 particles interaction with dislocations and impediment of crack during loading may also improve strength [Sharma et al., 2019, Dieter and Bacon, 1986]. Hardness (Fig. 3.9(b)) increases with increase in hard particles. Further, high dislocation density due to lattice mismatch also increases the hardness of the composites. Difference in the coefficient of thermal expansion of ZrB_2 particles and matrix is also a contributing factor [Dieter and Bacon, 1986, Ramesh et al., 2019].

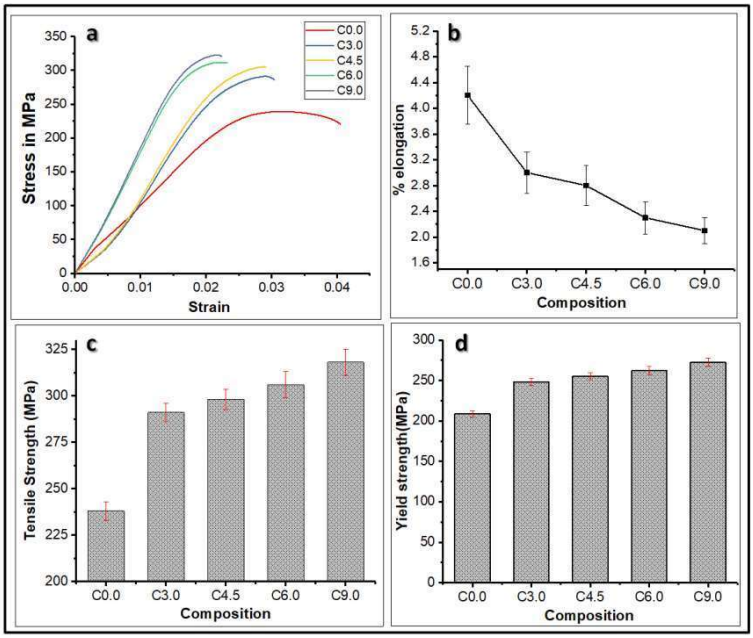

Fig. 3.8 Behaviour of ZA alloy and composites (a) Stress-strain curve (b) % Elongation (c) Ultimate tensile strength (MPa) (d) Yield Strength (MPa) [Vineet et al., 2019]

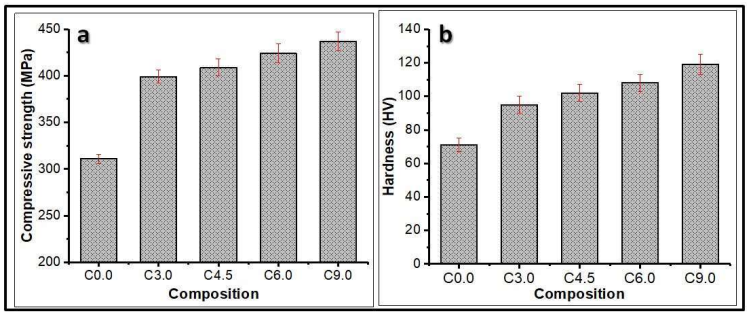

Fig. 3.9 Behaviour of ZA alloy and composites (a) Compressive strength (MPa) (b) Hardness (HV) [Vineet et al., 2019]

3.8 ZA/ZrB_2 COMPOSITES AS BEARING MATERIALS

There are many materials which are widely used as bearing materials such as conventional Cu-Sn based bronze, Fe based bronze, Al based bronze and Fe-Gr (graphite) based bronze [Tavakoli et al., 2008, S.R. Kumar et al., 2018, Parveej et al., 2021, Savaskan et al., 2008]. Therefore, to check the suitability of the developed material as bearing, the

mechanical properties of the present composites are also compared with these widely used materials. For the comparison purpose, strength to weight ratio and hardness to weight ratio of the materials are used.

Figure 3.10 shows the comparison of mechanical properties of ZA alloy, composites and bearing materials. Figure 3.10(a-b) clearly reveal that despite using liquid metallurgy the ZA alloy and ZA base composites show significant improvement in strength to weight ratio over pre-existing Cu-10Sn alloy journal bearing materials prepared using PM method. This difference becomes more prominent when it is compared with conventional bearing material like SAE 660 and SAE65 etc. Figure 3.10(c) shows the comparison of hardness to weight ratio for ZA alloy and composites with various other bearing materials. Barring one case, ZA/ZrB_2 composites continue to show their superiority in all other materials taken for comparison [Vineet et al., 2022(a)].

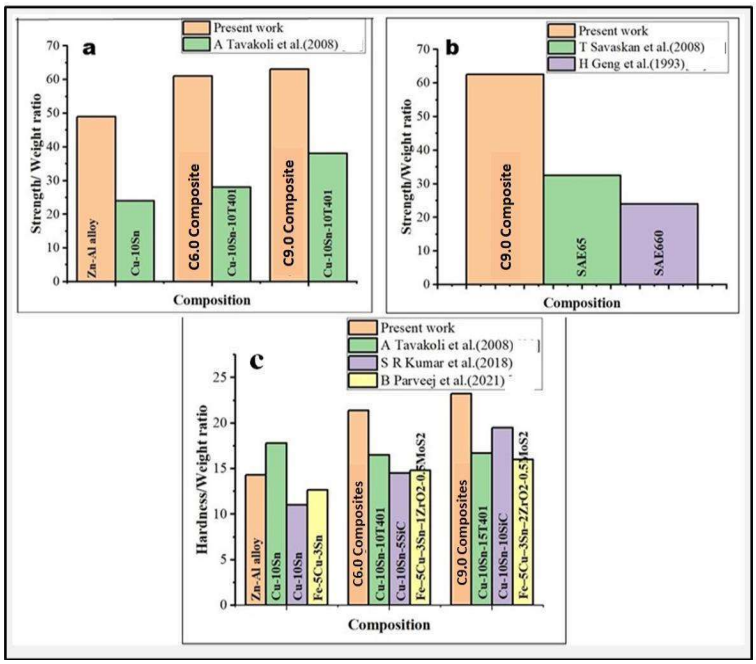

Fig. 3.10 Comparative study of ZA/ZrB_2 composites and bearing materials (a-b) Strength to weight ratio and (c) Hardness to weight ratio [Vineet et al., 2022(a)]

3.9 CONCLUSIONS

The ZA/ZrB_2 *insitu* composites could be successfully fabricated using stir casting technique. Increment in vol.% of ZrB_2 (0, 3, 4.5, 6, and 9) led to the following conclusion from this study:

- *Insitu* formation of ZrB_2 particles causes grain refinement of the matrix and this refinement increases up to about 54% at 9 vol.% of ZrB_2.
- SEM images reveal that *insitu* reaction led to largely uniform distribution of ZrB_2 particles and majority of the particles lie between 0.3 to 0.9 μm. Finer particles cause clustering of particles.
- The tensile strength of ZA alloy increases from 238 to 321 MPa at 9 vol.% ZrB_2.
- The compressive strength of ZA alloy increases from 311 to 433 MPa at 9 vol.% ZrB_2.
- The Vickers hardness of ZA alloy increases from 71 to 119 VHN at 9 vol.% ZrB_2.
- The higher strength to weight ratio and hardness to weight ratio with establish bearing materials suggest that ZA/ZrB_2 composites could be a good candidate for bearing applications.